Controlled atmosphere vibrating thermo-magnetometer (CatVTM): a new device to optimize the absolute paleointensity determinations

Thierry Poidras, Pierre Camps, Patrick Nicol

Controlled atmosphere Vibrating Thermo-Magnetometer (C_{at}VTM) : A new device to optimize the absolute paleointensity determinations

Thierry Poidras* Pierre Camps† Patrick Nicol

Abstract

The laboratory of paleomagnetism of Montpellier (France) developed a new one-axis Vibrating Thermal Magnetometer dedicated to the study of physical properties of natural rocks remanence. Among its key characteristics, this apparatus allows both to measure the magnetization moment on the interval from the room temperature to 700°C with a precision of $2x10^{-9}$ Am^2, and to acquire a total or a partial TRM using a steady field from -100 up to 100 μT. Another point that is worth noting is that one can apply a controlled atmosphere by means of argon flux in order to prevent oxidation of the studied sample during heating. In the present paper, we report a technical description of this new instrument and review some specific applications in absolute paleointensity surveys.

1 Introduction

In 1994, the paleomagnetic laboratory in Montpellier bought a vibrating magnetometer with translation manufactured by Orion (Borok, Russia). The principal characteristic of this one-axis magnetometer is to measure continuously, during heating-cooling cycles between the room temperature and 700°C, the remanent magnetization recorded in rock samples of $\sim$1 cm^3 size. A second specification is that continuous measurements are carried out either in a null magnetic field (demagnetization curve) or in presence of a weak-magnetic field between -100 and +100μT applied along one axis of the sample (magnetization curve). It is obvious that such apparatus is of great interest in paleomagnetic surveys since it allows to test directly the physical properties of the Natural Remanent Magnetizations (NRM). In particular, it opens new prospects in different fields such as:

1. The selection of well-suited samples for paleointensity determinations [1, 2].
2. The development of new methodologies in paleointensity [3, 4].

*Géosciences Montpellier, CNRS and University of Montpellier, France
†Corresponding author (e-mail: camps@gm.univ-montp2.fr)

3. The experimental investigation of physical properties of thermo, thermo-viscous, and chemical remanent magnetizations, according to the size of magnetic minerals [5, 6].

Unfortunately the former apparatus was failing in term of reliability, since we encountered multiple breakdowns of various origins, and unsatisfactory in term of sensitivity especially at high temperature, since some slightly magnetized basalts could not be analyzed. Consequently, during more than 10 years, we have worked on its development and upgrade with the objective to improve both its reliability and its sensitivity. Today, we have a new prototype called C_{at}VTM in which only the detecting coils and the field application coils are of origin. This apparatus supplement the list of laboratory-made magnetometer, dedicated to rock magnetic studies, able to measure magnetic moments at elevated temperature [see 7, for a review].

In the first part of the present paper, we will report a technical description of Montpellier instrument by emphasizing its technical characteristics. Next, we will review some specific applications in absolute paleointensity surveys. Finally, we will conclude on what could be its future developments.

2 Magnetic Moment Measurement in a Vibrating Magnetometer

The principle of a vibrating magnetometer is to measure a voltage induced in a pick-up coil assembly by a changing magnetic flux. Usually, the changing flux is achieved by a periodically change of the sample position along the vibrating axis within a fixed detecting coil assembly. The motion of a magnetic sample produces a magnetic flux through the coil as:

$$\Phi_B = \mathbf{G} \cdot \mathbf{M}$$

where Φ_B is the magnetic flux in Webers, $\mathbf{G}$ is the vectorial geometry factor in $\mathrm{Wb/Am^2}$, and $\mathbf{M}$ is the magnetic moment of the sample in $\mathrm{Am^2}$. The voltage induced in the coils by the change in times of the magnetic flux is given by the Faraday's law of induction:

$$v = -\frac{d\Phi_B}{dt}$$

where v is the voltage in volts, and t is the time. For vibrating magnetometer with a linear translation of $\mathbf{M}$ following z-axis, an oscillatory voltage is generated as:

$$v = -\mathbf{M}\,\frac{d\mathbf{G}}{dz}\,\frac{dz}{dt}$$

This equation helps us to identify three important parameters to achieve the best measurement performances. The first is the sample signal $\mathbf{M}$, which is the sum of the remanent magnetic moment of the sample $\mathbf{M_r}$ and an induced moment $\mathbf{M_i}$ which is only present if a residual magnetic field exists in the measurement zone. Provided that $\mathbf{M_i}$ is negligible, there is nothing we can do on sample signal except to choose a sample volume as large as possible. The second, and certainly the most important, is the variation of the vectorial geometry factor along the vibrating axis ($d\mathbf{G}/dz$). This term characterizes the dependence of

the signal induced in the coils upon the sample-coil system geometry. The third represents the sample motion (dz/dt). It depends on the quality of the mechanical system and on its control. In a vibrating magnetometer, the sample undergoes a sinusoidal vibration such as:

$$z = z_0 + a \ \cos(\omega t)$$

where z is the sample position along the vibration axis, a and ω are the amplitude and the angular frequency of the vibrations, respectively, and z_0 is the distance between the center of the motion and the center of the coil assembly. Then, we have:

$$\frac{dz}{dt} = a\omega \ \sin(\omega t)$$

This equation clearly shows that, for a given sample magnetic moment, a larger vibration amplitude a as well as a higher frequency of vibration ω will increase the voltage induced in the coils, and thus will increase the magnetometer sensitivity.

3 C_{at}VTM: Description and Solutions

The C_{at}VTM magnetometer is a horizontal assembly composed by several main parts described hereafter and illustrated on Figure 1.

3.1 The sensor assembly

We kept the sensor assembly of origin as manufactured by the Orion company (Borok, Russia). This assembly is made of two coils in series-opposition centered in two concentric mumetal shields. Their physical characteristics are as following:

- Outer(Inner) coil diameter: 74.8(37.8) mm
- Coil width: 17 mm
- Outer(Inner) mumetal shield: 164(144) mm length and 100(77) mm diameter.
- Resistance of the two coils in series: 14955 Ω
- Wire diameter : 0.11 mm.

3.1.1 $\mathbf{G}(z)$ profile determination:

The knowledge of the vectorial geometry factor along z-axis is fundamental to fully describe the sensor assembly. The main reason is practical: the zone in which the sample is translated must be chosen such as $d\mathbf{G}/dz$ be as constant as possible over all the sample volume during its movement. We determined the $\mathbf{G}(z)$ profile by means of two different approaches. The first was to solve numerically the analytical solution for our sensor assembly geometry (see Appendix A). The second was to measure experimentally this profile. This is simply done by measuring the magnetic field generated along the vibrating z-axis when the

sensor coil assembly is supplied with a known current I. $\mathbf{G}(z)$ profile is then estimated using the relation :

$$\mathbf{B}(z) = \mathbf{G}(z) \cdot \mathrm{I}$$

where B is the magnetic induction in Tesla, and I the current passing through the wires in Ampere. We designed and built a specific probe to achieve this measurement. This probe is described in section 3.2. We find, using a 0.01 mA DC current, a maximum field of 4.15 μT for z = -23.5 mm and a minimum field of -4.15 μT for z = 23.5 mm. The zone where $(d\mathbf{G}/dz)$ is nearly constant and offers a good range for sample motion is bounded between -13 mm and 13 mm. Over this amplitude range, the slope of $(d\mathbf{G}/dz)$ is 26.21 T/Am (Figure 2). Setting the value of the vibration amplitude a to 8.14 mm and the vibration frequency f to 8 Hz, with $\omega = 2.\pi.f$, we can calculate a peak-value of 0.4092 m/s for (dz/dt). Then, the value of the magnetic moment measured by the lock-in amplifier (model SR830) and the preamplifier is:

$$\mathbf{M_{rms}} = -\frac{1}{K} \times \frac{v_{rms}}{(d\mathbf{G}/dz)\ (dz/dt)}$$

with,

$$\mathbf{M_{rms}} = \frac{\mathbf{M}}{\sqrt{2}}$$

where $\mathbf{M_{rms}}$ is the root mean square of the magnetic moment in Am^2, K is the gain of the preamplifier, here K=6675, and $\mathbf{M}$ is the sample magnetic moment.

3.1.2 Offset and Noise:

The output of the lock-in amplifier v_{rms} is given by:

$$\begin{aligned} v_{rms} \quad = \quad & vp_{offset} + vp_{noise} \\ & + K\big[- (\mathbf{M_m}).(d\mathbf{G}/dz).(a_m\omega_m)/\sqrt{2} \\ & + vs_{noise}\big] \end{aligned}$$

where vp_{offset} and vp_{noise} are the constant offset and the constant noise of the preamplifier, respectively, K is the gain of the preamplifier, $\mathbf{M_n}$ is the measured magnetic moment ($M_m = M + M_{noise}$), a_m is the amplitude of the vibration ($a_m = a + a_{noise}$), ω_m is the circular frequency ($\omega_m = \omega + \omega_{noise}$), and vs_{noise} is the Johnson noise of the sensor coils. The offset and noise determinations were achieved experimentally using first a vibrating coil with no current (I=0 A) giving a null magnetic moment (M=0 Am^2). Setting I=0 A, we have:

$$v_{rms} = vp_{offset} + vp_{noise} + K.vs_{noise}$$

The experiment lasted 20 minutes during which 776 data were acquired. We averaged the 20-mn-signal by calculating the arithmetic mean, and found 66±47 μV. The mean value corresponds to the offset of the preamplifier, while the standard deviation is the noise of the preamplifier plus the amplified noise of the sensor. A value of 47 μV corresponds to 0.6x10^{-9} Am^2_{rms} or 3.1x10^{-9} Am^2 peak-to-peak noise. Then, since the noise depends on the magnetic moment, we repeated the same experiment for different values of current through the calibration coil.

3.1.3 Johnson noise:

The detection coils produce a Johnson noise, generated by the thermal agitation of electrons, which happens regardless of any applied voltage. The rms value of the voltage across a resistor due to the Johnson noise, expressed in volts per root hertz, is given by:

$$\nu_n = \sqrt{4k_bTR\Delta f}$$

where k_B is the Boltzmann's constant in joules per kelvin, T is the coil temperature in kelvins, R is the resistor value in ohms, and Δf is the bandwidth in Hertz over which the noise is measured. The amount of noise measured by the SR830 lock-in amplifier is given by:

$$v_{noise} = 0.13\ \sqrt{R\ W}$$

where v_{noise} is the rms voltage in nVolts, R is the resistance of the sensor coil system, and W is the equivalent noise bandwidth of the SR830 low-pass filter. In our vibrating magnetometer, with R = 14955 Ω and W = 0.026, the minimum rms-noise we could achieve is theoretically 2.56 nV. This value corresponds to 0.34x10^{-9} A.m^2 or 1.7x10^{-9} A.m^2 peak-to-peak noise as notified in the SR830 manual (page 3.17).

3.1.4 Calibration:

As shown on Figure 2, harmonic distortions are suspected because $(d\mathbf{G}/dz)$ is not perfectly constant over the amplitude range. We quantified the rate-distortion D of the output waveform for two vibration amplitudes, 8.14 and 3.61 mm peak-values, keeping the vibration frequency at a constant value of 8 Hz. Results are presented in Table 1 for the first five harmonics. Note that a value of 8.14 mm is preferred for a general use, although the rate-distortion is higher than for a value of 3.61 mm, because the corresponding $(d\mathbf{G}/dz).(dz/dt)$ is higher (10.72 compared to 4.75). Then, one needs to calibrate the sensor in order to compensate the system non-linearities.

One way to perform the calibration is to build a dedicated coil. Paperno et al. [8] described how to design a cylindrical induction coil to accurately simulate an ideal magnetic dipole. The calibration coil we built is 6.35 mm length and 9.5 mm diameter. This coil produces a magnetic moment of 1.488x10^{-3} A.m^2 for one Ampere. An alternative solution is to perform a cross calibration between our 2G cryogenic magnetometer and the C$_{at}$VTM by measuring on both systems a remanent magnetization imparted to a sample in the laboratory. This double measurement is repeated for several steps of AF-demagnetization until the limits of the C$_{at}$VTM are reached.

3.1.5 Signal-to-noise ratio:

We use our calibration coil to determine the signal-to-noise ratio (STN). Each experiment lasts 20 minutes during which a constant current is applied. STN is given by:

$$STN = 20\ \log\left(\frac{v_{signal}}{v_{noise}}\right)$$

where v_{signal} is the average of the output voltage, and v_{noise} is the corresponding standard deviation. It is usually admitted that measurements with a signal-to-noise ratio lower than 10 dB are inexploitable. Results reported in Table 2

show that meaningful measurements can be performed from a sample magnetic moment as low as $2x10^{-9}$ Am^2 (15dB). These results take into account the modulation "noise" induced by the variation of amplitude, which is estimated to be about ± 50 μm from the equation in section 3.1.2, and by the variation of frequency, which is $f_n = \pm$ 0.001 Hz.

3.1.6 Others sources of noise:

Additional noises on magnetic moment measurements are due to the resistive heater and to the solenoid applying the field on the sample. These noises are difficult to be estimated. During heatings, the physical and chemical properties of the magnetic minerals may suffer from changes. These variations can be considered as a noise in the way that we loose informations in the signal due to uncontrolled changes in the magnetic properties of the sample.

3.2 Magnetic shielding

The pick-up system is surrounded by two mumetal magnetic shields which provides a low reluctance path guiding the magnetic field around the measurement zone. An accurate estimation of the residual field is required. As the furnace inner diameter is only 17 mm, it is not obvious to measure the three components of the residual field in the measurement zone. We designed and built a specific 3-axes probe in order to achieve this measurement. We choose the Honeywell sensors HMC1001 and HMC1002. Those magnetoresistive sensors are able to detect a magnetic field as low as 3 nT for a frequency of 10 Hz. The sensors are mounted on a printed circuit board. Sensors control, signal acquisition and data processing are achieved with the MSC1211 component from Texas Instruments. The MSC1211 is a precision 24-bit analog-to-digital converter (ADC) with a 8051 microcontroller. This probe is a standalone system that can be used to measure the magnetic field for other needs in the laboratory.

The shielding factor or effectiveness S is defined as the ratio of the external field to the residual field within the shielded zone. Our system yields a good attenuation, S being measured between 175 and 250. Despite the mumetal magnetic shield, the field in the measurement zone is not totally cancelled. To obtain better results the system is positioned so that its axis be perpendicular to the ambient magnetic field. However there is still a little field measured between 100 and 200 nT which has to be cancelled.

3.3 Field application coils

A solenoid located between the pick-up coils and the sample enables the user to apply a field along the sample z-axis. This same solenoid is used to apply an offset to obtain a residual field as little as possible when a null field is required. The quality of the current source is a decisive factor. We use a National Instruments Digital to analog card followed by a voltage to current amplifier to drive the z-coil. It also appears that the transverse field in the measurement zone is not null and can be quite important depending on the quality of the mumetal shielding. We encountered problems with induced magnetization caused by this field. Two perpendicular Helmholtz coils assembly are wound between the magnetic shield and the pick-up coils to cancel this field. Two sources supply a small

current to each coil to nullify the two components of the transverse field.

3.4 Sample Heater

The heating of samples is one part of the system to which we have to give attention. It is a resistive furnace made of a bifilar winding that is non-inductive in a theoretical point of view. We have to pay attention on how to wind in order to achieve the non-inductivity and to offer an homogeneous temperature profile in the measurement zone. The furnace is wound with Nikrothal 80 non-magnetic wire on a quartz tube of 17 mm inner diameter and 20 mm outer diameter. The total resistance is 75 Ohms and the maximum current is two amperes. A copper jacket and a thin layer of rockwool insulate the heater from the resistor coils. The jacket is designed so that the cooling liquid flow be regular on its whole length. The cooling circuit is closed-looped and the flow rate is regulated at 0.6 l/h. If for any reason the flow rate is to low, the security switches down the power supply. The power supply, designed and self-built in the laboratory, is a Pulse Width Modulation (PWM) supplied with a 150 V voltage-source. It is a full H-Bridge which enables a bi-directional current flow in the resistor wire. The specificity of this PWM power supply is that each current pulse is reversed, in order to minimize the effect of the imperfect non-inductive winding. The period of the PWM is 1 Khz. The temperature is measured with a thermocouple type E (-200°C to 900°C) or type S (0°C to 1450°C). The thermocouple is part of the sample holder and its exposed part is in direct contact with the sample. We use a Eurotherm controller to program the ramp rate and dwelling temperature needed to control the heating process.

3.5 The Sample Holder

The sample holder is made of three ceramics parts (Figure 3): the holder by itself is made in Macor. This machinable glass ceramic has a continuous use temperature of 800°C and a peak temperature of 1000°C. Its coefficient of thermal expansion readily matches most metals and sealing glasses. It exhibits zero porosity, and unlike ductile materials, wont deform. It is an excellent insulator at high voltages, various frequencies, and high temperatures. This holder minimizes the heat loss out of the heater.
The bell that maintain the sample is made of Shapal. It is a machinable form of Aluminium Nitride ceramic with excellent mechanical strength and thermal conductivity. Shapal has zero porosity, good abilities to seal under vacuum, low thermal expansion coupled with a high heat resistance. Shapal also offers excellent machinability with conventional machine tools. The machined Shapal-bell (female) is screwed on the male screw thread of the Macor-holder. During the experiment they join together with a bond made of water and kaolin. We use some rockwool in the assembly to avoid direct contact between the sample and the bottom of the bell. Inside the Macor-holder, there is a ceramic rod (two holes) that contains the thermocouple.

A gas flow (argon) is sent through a hole at the base of the Macor-holder and get out of the Shapal-bell through a little hole. The flow is tuned at the flowmeter to be as the smallest rate as possible ($\sim$ 0.05 l/mn). An electrical valve is driven by the computer to shut off the gas supply at the end of the

experiment. A 70-cm-long fiber carbon rod is used to connect the sample holder to the motor.

3.6 Sample Motion Generator

As seen previously, the stability of both amplitude and frequency of the sample displacement is required to achieve a good measurement. This is why we used a linear motor. We chose the ThrustsTube Micro Motor model TB1104 from Copley Motion Systems. The mass of the system (forcer mass + sample holder + transmission rod) limits the speed performances of the assembly. The motion of 16.14 mm peak-to-peak at 8 Hz is a compromise we chose between sensitivity and long-time performance. Actually, some experiments can last more than 30 hours. The motor forcer moves along the axis of the thrust rod mass (Figure 4). It is heavier than the thrust rod mass but, as the thrust rod, is strongly magnetized and thus it has to be steady. The forcer is fixed to a low profile guide system. The carbon rod connected to the sample holder is fixed at the extremity of the system. The mechanical assembly has to be as simple as possible. We use to minimize the friction a miniature Drylin (linear bearing) system from Igus©. The two floating bearings used to guide the motor are very light and have a very low coefficient of friction. The mobile forcer is fixed to a plate to transmit the motion to the fiber carbon rod. A linear optical encoder module reads the position on a linear scale fixed on the mobile assembly. The resolution of the encoder assembly is 8.8 μm. We use a DC brushless digital servo-amplifier to drive the motor and program the sample displacement. The servo-amplifier is configured via a three-wire, full-duplex RS-232 port, by means of the CME2 software or with specific commands. The servo-amplifier provides a function-generator command to configure the amplitude and frequency of the motion. The stability of the vibration is $\pm$ 0.001 Hz for the frequency and $\pm$ 50 μm for the amplitude .

3.7 Signal Processing

As the pick-up coil assembly has a high resistance (15 KΩ) it behaves more than a current source than a voltage source. Thus, we used a current to voltage preamplifier followed by a low-pass filter. The output of the preamplifier is directly connected to a lock-in amplifier SR830 (Stanford Research System). The reference input comes from a photo-electric detector which is mounted on the motor assembly.

3.8 Data Processing

Labview is used to configure the experiment and to process the data. The computer drives the temperature controller, the applied field, the motor servo-amplifier and the lock-in amplifier through the GPIB bus. Before to run the experiment, the user has to define a succession of temperature and applied field profiles. Each profile consists of a heating or cooling ramp rate (with field to apply) and the temperature to reach (with field to apply). There is no limitation in the number of profiles. During the experiment it is possible to remove or add a profile.

At the end of each profile the magnetization at the dwell temperature is computed. Each profile has its own datafile on which it is possible to work during the experiment. As soon as the experiment is finished, the results are available and can be plotted and analyzed.

4 Applications in Absolute Paleointensity Determination by the Thellier Method

4.1 The Paleointensity method and its limitations

The principle of absolute paleointensity determination with Thellier type experiments [9] rests on the modeling of the natural remanent magnetization (NRM) by an artificial thermo-remanent magnetization (TRM) acquired in the laboratory in presence of a known magnetic field **H**. Indeed, the methods are based on a direct comparison between the stepwise thermal demagnetization of the NRM and the acquisition of partial TRM (pTRM). Various aspect of the method applicability have been widely discussed [see 10, for a review and a description of the original Thellier method and its derivatives]. To be brief, igneous rocks used for paleointensity determinations must satisfy the following three conditions :

1. NRM must be a TRM not disturbed by significant secondary components.

2. The magnetic properties of the samples must be reasonably stable during the laboratory heating.

3. Thellier method is based on three assumptions concerning the properties of pTRM usually referred to as the Thellier laws [11] which are valid only for fine remanence carriers, i.e. single-domain (SD) or small pseudo-single-domain (PSD) grains:
   (i) Additivity law: let two pTRMs imparted in the same magnetic field, pTRM(T_1,T_2) being acquired in the temperature interval T_1-T_2 and pTRM(T_2,T_3) being acquired in the temperature interval T_2-T_3 with $T_1 > T_2 > T_3$ then,

   $$\mathrm{pTRM}(T_1, T_2) + \mathrm{pTRM}(T_2, T_3) = \mathrm{pTRM}(T_1, T_3)$$

   (ii) Independence law: the blocking and unblocking temperatures of pTRMs must be equal. This means that a pTRM(T_1,T_2) is not thermally demagnetized when heated in zero field at a temperature lower than T_2, while it is totally demagnetized when heated in zero field at a temperature equal or upper than T_1.
   (iii) The intensity of a pTRM(T_1,T_2) should not depend on the thermal history of the sample. This property can be checked for instance by comparing two different kinds of pTRM: a $\mathrm{pTRM}_a(T_1,T_2)$ acquired when the upper temperature T_1 is reached by cooling from Curie Temperature (T_c), i.e. from above, and a $\mathrm{pTRM}_b(T_1,T_2)$ when T_1 is reached by heating from T_{room}, i.e. from below [12, 13]. If the pTRMs are independent of the thermal history of the rock sample then,

   $$\mathrm{pTRM_a}(T_1, T_2) = \mathrm{pTRM_b}(T_1, T_2)$$

It is obvious that Thellier type experiments impose severe conditions on the samples that are rarely encountered in natural rocks. A direct consequence is that paleointensity determinations are very often characterized by a high failure rate, ranging between 70 and 90% [14]. Hence, the number of determinations of absolute paleointensity available is extremely weak: To date approximately 3000 data, representative of instantaneous recordings of the paleomagnetic field, were published for the whole geological times. In addition to the low number of data available, their quality is unequal: 63% of the published data are eliminated with criteria of selection particularly not very severe and, in particular, almost all the determinations between 4 and 60 Ma [15].

One of the specific purpose of using the C_{at}VTM in Montpellier is to test directly the physical properties of NRM in order to provide a relevant preselection of samples that can be successfully used for a paleointensity determination. Examples of simple tests carried out to this end are reviewed hereafter.

4.2 Is the NRM a pure TRM ?

A positive answer to this question is the first prerequisite for obtaining a paleointensity. Usually, authors used directional arguments to detect the presence of significant secondary component in the remanence, as the grouping of NRM direction in the same cooling unit associated with a careful examination of the individual vector end-point diagrams obtained during the demagnetization in the paleodirection study. This question may be answered more directly by means of our C_{at}VTM, provided that no noticeable chemical changes in the ferrimagnetic minerals occurred during the laboratory heatings. The experimental approach consists in comparing the shape of the continuous thermal demagnetization curve of the NRM with that of an artificial total TRM, imparted in a laboratory field **H** during the cooling from T_c to T_{room} on the same sample or on a sister sample from the same core. In this experiment, samples have to be drilled in the direction of the characteristic NRM due to the C_{at}VTM limitation of measurement along a single axis. A similar shape of these two continuous demagnetization curves is a qualitative evidence that the NRM is actually a TRM (Figure 5)[1, 2]. This involves as a corollary that a difference between the two curves suggests that the NRM is not a pure TRM, which is a sufficient condition to turn down samples from the selection. Moreover, the demagnetization curve of the NRM yields an estimate of the unblocking temperatures of NRM, which is a valuable information to choose the heating steps in the Thellier experiment.

It is obvious that a positive result in this experiment proves not only that the NRM is a TRM but also that the nature and/or the physical properties of the Fe-Ti oxides carrying the magnetization are not altered during heatings. Thus, condition 1 and condition 2 as stated above are checked simultaneously. In practice, the thermal stability is first verified independently by continuous measurements of magnetic susceptibility in weak field according to the temperature (KT curves). In Montpellier, we use the susceptibility meter Kappabridge KLY3© associated to the furnace CS3, in which the heating-cooling cycles are performed under Argon flux in order to limit oxidation of the ferrimagnetic minerals. Because we believe important in the sample selection procedure to keep constant the experimental conditions, NRM and TRM demagnetization curves are measured in the C_{at}VTM also under Argon flux.

4.3 Bolshakov and Shcherbakova's pTRM-tail test

The next step in sample selection for paleointensity determination is to assess the magnetic domain size in order to keep only sample with SD-like pTRM behavior. As stated in condition 3, the presence of multi-domain grains will invalidate the Thellier method. Usually, the size of the grains is estimated by the measurement of the hysteresis loop parameters for the whole rock. However this measurement often gives ambiguous answers between a behavior of PSD grain of that of a mixture of single- and multi-domain grains. Bolshakov et al. [16] were the first to suggest that the domain structure can be inferred from a thermomagnetic criterion. This test, illustrated on Figure 6, consists of a direct verification of the Thellier law of independence of pTRM which implies that any pTRM(T_1,T_2), with $T_1 > T_2$, must be entirely destroyed when heated en zero field strictly in the interval T_2-T_1. From an experimental study on synthetic powders of magnetite and hematite of various sizes, Shcherbakova et al. [13] defined the A parameter by

$$A(T_1, T_2) = \frac{\text{tail}[\text{pTRM}(T_1, T_2)]}{\text{pTRM}(T_1, T_2)} \times 100\%$$

as the relative intensity measured at room temperature of the pTRM remaining after heating to T_1 (pTRM-tail). According to this experimental study, this parameter can serve as a quantitative indicator of the domain structure of a sample. They found thresholds as following : the remanent carrier are predominantly SD grains for $A(T_1, T_2) < 4\%$, they behave as pseudo-single domain (PSD) grains for $4\% < A(T_1, T_2) < (15 - 20)\%$, and they are predominantly MD grains for $A(T_1, T_2) > 20\%$. A major drawback of the Bolshakov [16]'s pTRM-tail test is the initial heating to the Curie temperature necessary to demagnetized the NRM prior to the pTRM acquisition. Thus, this test can be applied only for samples thermally stable.

The main application of determining the parameter A is usually to screen out samples ill-suited for paleointensity determinations [see 1, 14, for example]. Shcherbakov et al. [17], arguing that this parameter is physically meaningful, even suggested to use it systematically before any paleointensity experiments. Further applications of A parameter have been proposed by Carvallo et al. [2] and Plenier et al. [18] to help in the interpretation of NRM-TRM diagrams. In their study, they measured the coefficient A at increasing temperature intervals and used the results to validate their choice of the most suitable portion of the NRM-TRM diagrams when, in non-ideal cases, two slopes yielding a technically acceptable determination are present. Whatever the use of the A parameter, its determination when possible strengthens the reliability of a paleointensity determination.

4.4 Pseudo-Thellier Paleointensity

Perrin [14] proposed a different approach to select suitable samples for paleointensity determination which do not required, as the pTRM-tail test, a total thermal demagnetization prior to the experiment. She proposed to perform using the C_{at}VTM a Thellier-like experiment with the sole objective to estimate the shape of the NRM-TRM diagram and therefore the temperature range where a

real Thellier experiment will be later performed. This method is called pseudo-Thellier because of the limitation of measuring the magnetization along one axis induces errors too much high to consider valid the paleointensity estimate. This conclusion remains true even if the small sample used in this experiment is drilled as close as possible along the characteristic NRM direction.

4.5 Shift of the Baseline in Thellier experiment

The idea is to perform a traditional Thellier [9] experiment except that the NRM left and the pTRM gained are measured at a temperature greater than the room temperature (for instance 200°C). Remanence measurements are classically performed at room temperature just for purely technical reasons: paleointensity oven and magnetometer are usually two different apparatus. We report here an example of application of this original method on Icelandic lava flows from Tjornes peninsula, which are suspected to have recorded the Matuyama-Bruhnes transition [19]. A very detailed rock magnetic study (low- and high-temperature susceptibility curves, Forc diagrams, thin sections analysis) revealed the joint presence of two titanomagnetite populations, the first, which has undergone a high temperature oxidation, shows a single-domain (SD) behavior and a mean curie temperature above 500°C, while the second, not oxidized, presents a multi-domain (MD) behavior and a mean curie temperature around 150°C [4]. The presence of MD grains does not enable us to obtain paleointensity estimates with a conventional method. However, by using the C_{at}VTM and by choosing a temperature of measurement higher than the Curie temperature of the MD population, e.g., 200°C, we obtained paleointensity diagrams of very good technical quality (Figure 7).

5 Conclusion

The C_{at}VTM is an apparatus which should improve the success rate in absolute paleointensity determinations by investigating directly the physical properties of the NRM carried by natural rocks. Its use allows to efficiently preselect well-suited samples for paleointensity experiments. Beyond this practical aspect, some experiments as the ones presented in this paper strengthen the reliability of the paleointensity estimates. This why we believe important to continue to work on further developments. To date, improvements can be made on each step of the measurement process. It is still possible to work on more sensitive coils system, and also on three-axis systems [20]. The use of a very low-noise preamplifier will improve the signal-to-noise ratio of the system by decreasing the noise at the source. As linear motors are also improving, it should be possible to speed up significantly the frequency of the sample motion. Another way to improve the signal-to-noise ratio is to increase the induced signal by going out of the low-frequency electronic noise area. The resistive heater is a important source of noise. It is an exciting challenge to find other ways to heat the sample by means of an external heat source as performed in the prototype of magnetometer developed by Wack et al. [7].

6 Acknowledgments

This work was initiated by Michel Prévot. He bought the original version of the vibrating magnetometer and did a lot of work to improve it. Without him the CatVTM would not have been built. His work is gratefully acknowledged. Reviews by Maxime LeGoff and Juan Morales helped to clarify several issues on the original manuscript and are much appreciated. We also benefited from discussions with Mireille Perrin and Brigitte Smith.

7 Appendix

A1: Analytical solution for $\mathbf{G}(\mathbf{z})$

We present here the analytical solution used to calculate the $\mathbf{G}(\mathbf{z})$ profile in the CatVTM. In this vibrating magnetometer, the sensor assembly is made of two coils in series-opposition (e.g., Smith's arrangement). The vectorial geometry factor is then:

$$\mathbf{G}(z) = \mathbf{G_1}(z) - \mathbf{G_2}(z)$$

where the subscripts 1 and 2 denote the first and the second coil, respectively. For the first coil, $\mathbf{G_1}$(z) is determined by means of the equation given by Durand [21]:

$$\mathbf{B}(\mathbf{z}) = J \cdot \frac{\mu_0}{2} \int_a^b (cos\gamma_1 \pm \cos\gamma_2) d\rho$$

where B is the magnetic induction in Tesla, J is the current density in A/m^2, a and b are the coil inner- and outer-radius in meters, respectively, and γ_1 and γ_2 two angles as illustrated on Figure 8. Then

$$\mathbf{G_1}(z) = \frac{\mathbf{B}(\mathbf{z})}{J}$$

is expressed in Tm^2/A. To be directly comparable with the experimental measurement shown on Figure 2, we use the relation

$$J = \frac{I_S}{S}$$

where I_S is the total intensity of current in amperes passing through the section S ($A_1B_1B_2A_2$ on Figure 8), and S is the surface of the section in m^2, $S = 2c(a-b)$, where 2c is the length of the coil. Thus, we obtain:

$$\mathbf{G_1}(\mathbf{z}) = \frac{\mu_0}{2 \cdot S} \int_a^b (cos\gamma_1 \pm \cos\gamma_2) d\rho$$

where $\mathbf{G_1}(\mathbf{z})$ is now in T/A, with $\mathbf{G_1}(z)$ positive if the point P is inside the limits of the coil (-c,c) and negative if P is outside the coil. This equation can be developed using:

$$\tan\gamma_1 = \frac{\rho}{z+c}$$

and,

$$\tan\gamma_2 = \frac{\rho}{|z-c|}$$

to obtain

$$\mathbf{G_1}(\mathbf{z}) = \frac{\mu_0}{2 \cdot S} \int_a^b \cos(\arctan(\frac{\rho}{z+c})) \pm \cos(\arctan(\frac{\rho}{|z-c|})) \cdot d\rho$$

$\mathbf{G_2}(\mathbf{z})$ is found using a translation between the centers of the two coils.

References

[1] P. Camps, G. Ruffet, V.P. Shcherbakova, V.V. Shcherbakov, M. Prévot, A. Moussine-Pouchkine, L. Sholpo, A. Goguitchaivili, and B. Asanidzé. Paleomagnetic and geochronological study of a geomagnetic field reversal or excursion recorded in pliocene volcanic rocks from Georgia (Lesser Caucasus). *Phys. Earth Planet. Int.*, 96:41–59, 1996.

[2] C. Carvallo, P. Camps, G. Ruffet, B. Henry, and T. Poidras. Mono Lake or Laschamp geomagnetic event recorded from lava flows in Amsterdam Island (southeastern Indian Ocean). *Geophys. J. Int.*, 154:767–782, 2003.

[3] A.B. Biggin and M. Perrin. The behaviour and detection of partial thermal thermoremanent magnetisation (ptrm) tails in Thellier palaeointensity experiments. *Earth Planets and Space*, 59:717–725, 2007.

[4] P. Camps, B.S. Singer, C. Carvallo, A. Goguitchaichvili, and B. Allen. Matuayma-Brunhes reversal on Tjornes Peninsula (northern Iceland) revisited. In *AGU Join Meeting*, Acapulco, MX, 2008. EOS.

[5] U. Draeger, M. Prévot, T. Poidras, and J. Riisager. Single-domain chemical, thermochemical and thermal remanences in a basaltic rock. *Geophys. J. Int.*, 166:12–32, 2006.

[6] A.B. Biggin and T. Poidras. First-order symmetry of weak-field partial thermoremanence in multi-domain ferromagnetic grains. 1. experimental evidence and physical implications. *Earth Planet. Sci. Letts*, 245:438–453, 2006.

[7] M. Wack and J. Matzka. A new type of three-component spinner magnetometer to measure the remanence of rocks at elevated temperature. *Earth Planets Space*, 59:853–862, 2007.

[8] E. Paperno and A. Plotkin. Cylindrical induction coil to accurately imitate the ideal magnetic dipole. *sensors and actuators*, 112(A):248–252, 2004.

[9] E. Thellier and O. Thellier. Sur l'intensité du champ magnétique terrestre dans le passé historique et géologique. *Ann. Geophys.*, 15:285–376, 1959.

[10] J-P. Valet. *Encyclopedia of Geomagnetism and Paleomagnetism*, chapter Paleointensity, Absolute techniques, pages 753–757. Encyclopedia of Earth Sciences. Springer, 2007.

[11] E. Thellier. Sur l'aimantation des terres cuites et ses applications géophysiques. *Ann. Inst. Physique du Globe, Univ. Paris*, 16:157–302, 1938.

[12] Y.K. Vinogradov and G.P. Markov. *Investigations in rock magnetism and palaeomagnetism*, chapter On the effect of low temperature heating on the magnetic state of multidomain magnetite, pages 31–39. Inst. of Phys. of the Earth, Moscow, 1989. (in Russian).

[13] V.V. Shcherbakova, V.P. Shcherbakov, and F Heider. Properties of partial thermoremanent magnetization in pseudosingle domain and multidomain magnetite grains. *J. Geophys. Res.*, 105:77767–781, 2000.

[14] M. Perrin. Paleointensity determination, magnetic domain structure and selection criteria. *J. Geophys. Res.*, 103(B12):30,591–30,600, 1998.

[15] M. Perrin and E. Schnepp. IAGA paleointensity database: distribution and quality of the data set. *Phys. Earth Planet. Int.*, 147:255–267, 2004.

[16] A.S. Bol'shakov and V.V Shcherbakova. A thermomagnetic criterion for determining the domain structure of ferrimagnetics. *Izv. Acad. Sci. USSR Phys. Solid Earth*, 15:111–117, 1979.

[17] V.P. Shcherbakov, V.V. Shcherbakova, Y.K. Vinogradov, and F. Heider. Thermal stability of pTRMs created from different magnetic states. *Phys. Earth Planet. Int.*, 126:59–73, 2001.

[18] G. Plenier, P. Camps, R.S. Coe, and M. Perrin. Absolute palaeointensity of Oligocene (24-30 Ma) lava flows from the Kerguelen Archipelago (southern Indian Ocean). *Geophys. J. Int.*, 154:877–890, 2003.

[19] L. Kristjansson, H. Johannesson, J. Eiriksson, and A. I. Gudmundsson. Brunhes-matuyama paleomagnetism in three lava sections in iceland. *Canadian Journal of Earth Sciences*, 25(2):215–225, 1988.

[20] M. Le Goff and Y. Gallet. A new three-axis vibrating magnetometer for continuous high-temperature magnetization measurements. *Earth Planet. Sci. Lett.*, 229:31–43, 2004.

[21] E. Durand. *Magnétostatique*, chapter 3, page 141. Masson et Cie, 1968.

Table 1: Measurements of rate-distortion

Harmonics f = 8 Hz	D % a = 3.61 mm	D % a = 8.14 mm
1.f	100	100
2.f	0.451	2.047
3.f	1.128	1.528
4.f	0.028	0.044
5.f	0.085	0.026
6.f	0.002	0.003
Total	1.218 %	2.555 %

Table 2: Signal-to-noise ratio

Moment Am2	Signal-to-noise dB
1.3e-9	8
1.9e-9	15
2.6e-9	21
6.5e-9	39
1.3e-8	52
1.45e-7	97
3.64e-7	99
1.46e-6	109

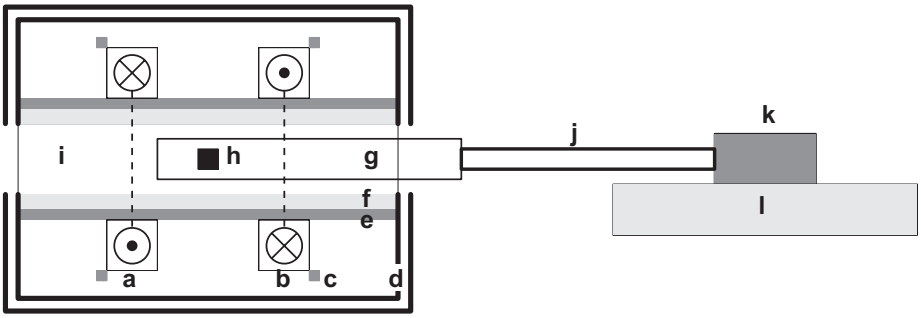

Figure 1: Schematic diagram of the C$_a$$t$VTM where a and b are the first and the second pick-up coil, respectively, connected in series opposition and perpendicular to the vibration axis, c is one of the X-Y field nulling coils, d is the 2-layers mumetal magnetic shield, e is the field solenoid, f is the woolrock insulation and water jacket, g is the sample holder with argon flow, h is the sample and the thermocouple, i is the heating coil, j is the carbon rod, k is the linear motor, and l is the linear bearing. Dashed lines are the connected parts of the same coils. The sketch is out of scale.

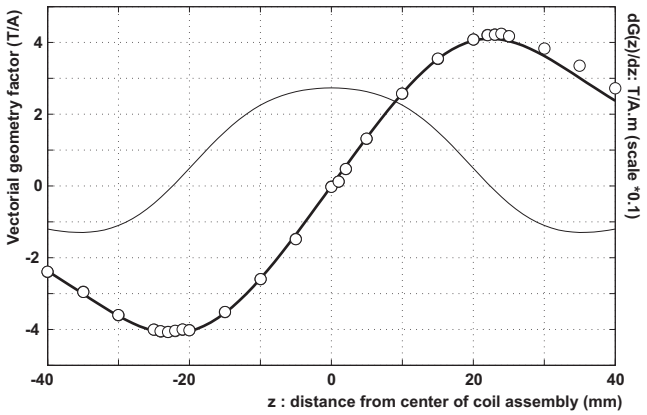

Figure 2: Vectorial geometry factor profile G(z). The calculate profile (bold curve) is compared to the experimental measures (open circles). The thin solid line is the calculated derivative dG(z)/d(z). z=0 corresponds to the center of the coil assembly.

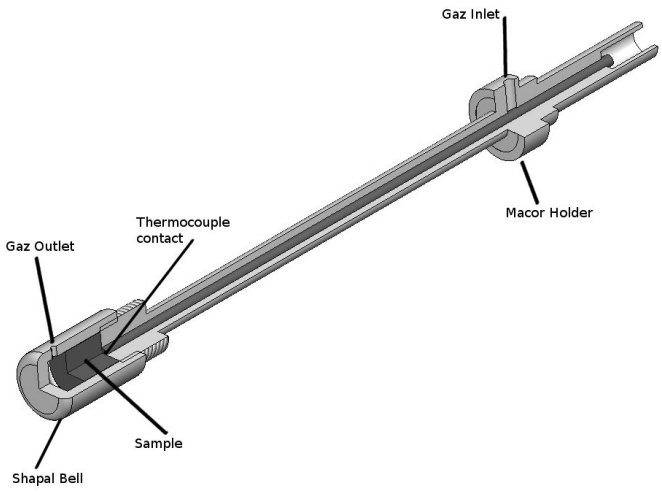

Figure 3: Sketch of the sample holder. Sample size is 1 cm^3.

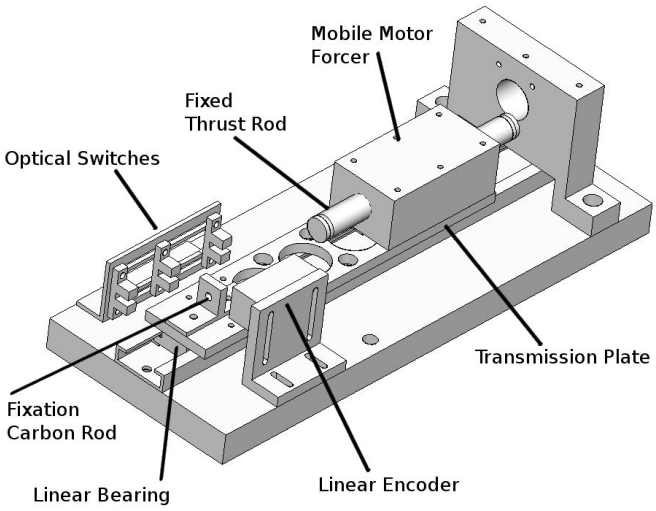

Figure 4: Sketch of the linear motor

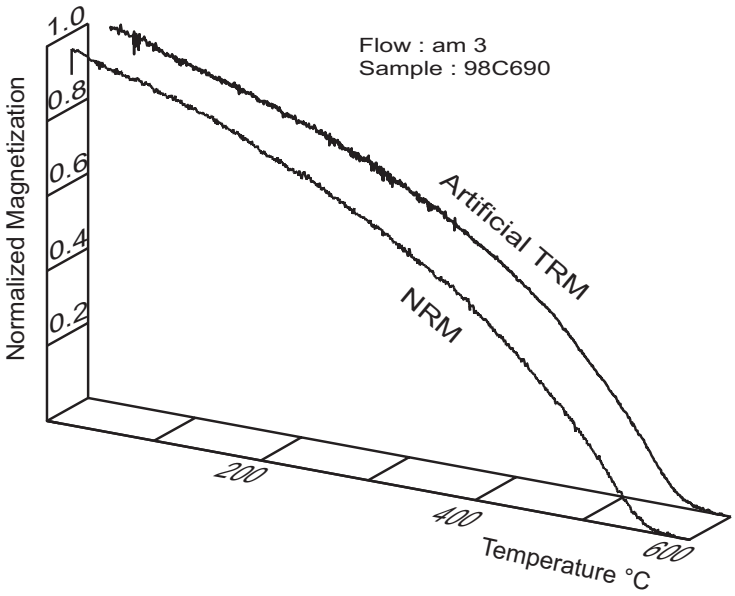

Figure 5: Continuous thermal demagnetization curves of NRM and artificial total TRM acquired in a 50-μT field for a lava sample from Amsterdam Island [2]. In the present case, the similarity between the two curves suggests that the NRM is a TRM.

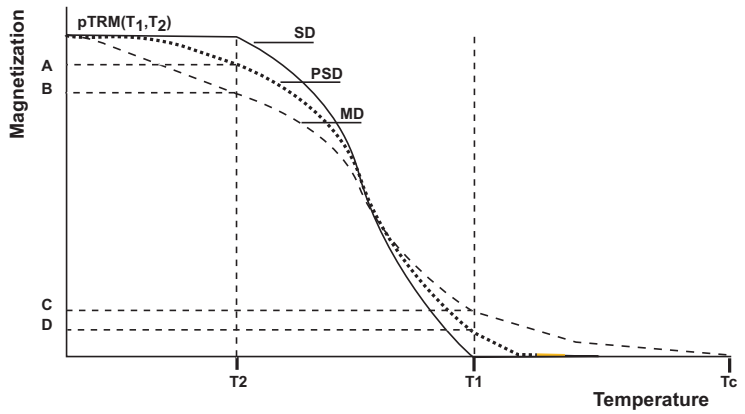

Figure 6: pTRM tail-check: Continuous thermal demagnetization of pTRM(T_1,T_2) illustrating two different pTRM-tails. The low-temperature pTRM-tail corresponds to the part of pTRM(T_1,T_2) removed at T2. The high-temperature pTRM-tail corresponds to the part of pTRM(T_1,T_2) unremoved at T1. A(B) is the low-temperature pTRM-Tail measured at room temperature for PSD(MD) grains. C(D) is the high-temperature pTRM-Tail measured at room temperature for PSD (MD) grains. Figure redrawn from Plenier et al [18].

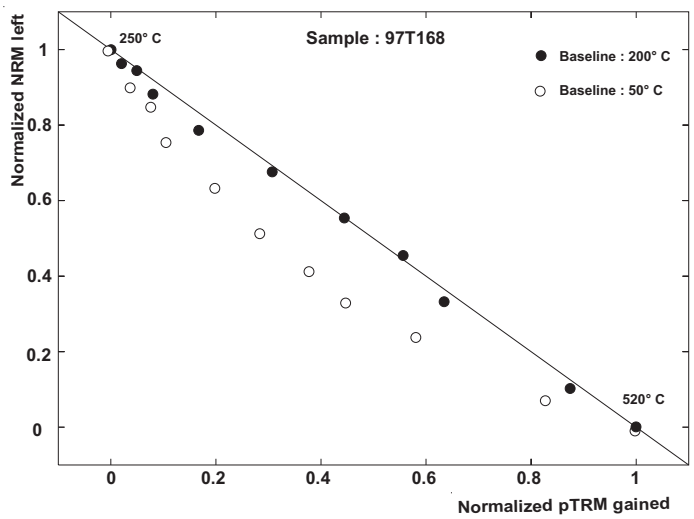

Figure 7: Comparison of two NRM-TRM diagrams obtained with the C_{at}VTM from two sister-specimens from the same core, where the remanences (NRM left, pTRM gained) are measured at 50°C (open circles) and at 200°C (filled circles). This basalt is characterized by a joint presence of MD grains with a Curie temperature of 150°C and of SD grains with a Curie temperature above 500°C. Measurements are performed under Argon atmosphere.

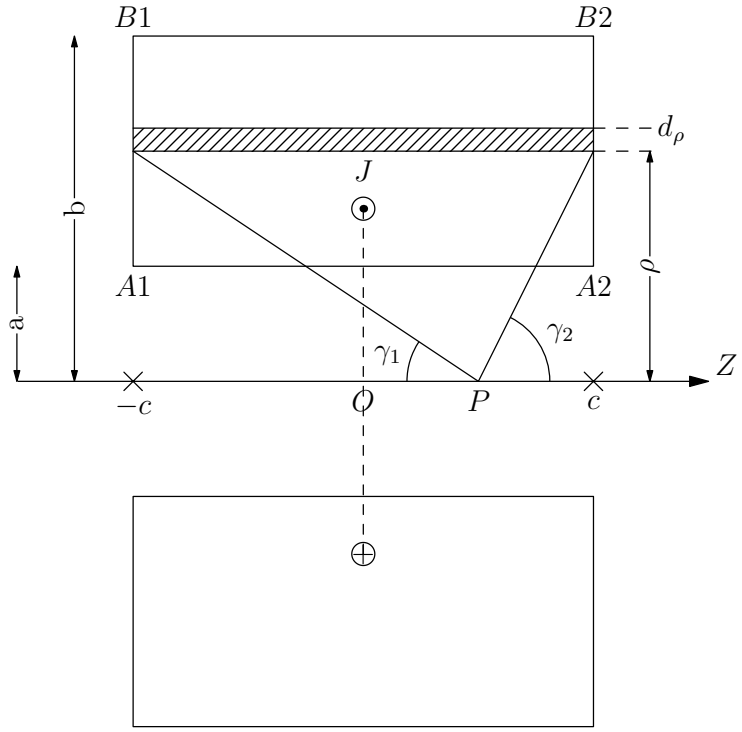

Figure 8: Thick coil cross-section illustrating the magnetic induction generated along the z-axis. a and b are the inner- and outer-radius of the coil of section S (A1-B1-B2-A2), respectively, c is the half-length.